GEOPHYSICS, VOL. 85, NO. 4 (JULY-AUGUST 2020); P. MR257–MR270, 9 FIGS., 4 TABLES.
10.1190/GEO2019-0074.1

Toward a better understanding of low-frequency electrical relaxation — An enhanced pore space characterization

Sabine Kruschwitz[1], Matthias Halisch[2], Raphael Dlugosch[2], and Carsten Prinz[3]

ABSTRACT

The relaxation phenomena observed in the electrical low-frequency range (approximately 1 MHz–10 kHz) of natural porous media such as sandstones are often assumed to be directly related to the dominant (modal) pore throat sizes measured, for instance, with mercury intrusion porosimetry. Attempts to establish a universally valid relationship between pore size and peak spectral induced polarization (SIP) relaxation time have failed, considering sandstones from very different origins and featuring great variations in textural and chemical compositions as well as in geometric pore space properties. In addition working with characteristic relaxation times determined in Cole-Cole or Debye decomposition fits to build the relationship have not been successful. In particular, samples with narrow pore throats are often characterized by long SIP relaxation times corresponding to long "characteristic length scales" in these media, assuming that the diffusion coefficients along the electrical double layer were constant. Based on these observations, three different types of SIP relaxation can be distinguished. We have developed a new way of assessing complex pore spaces of very different sandstones in a multimethodical approach to combine the benefits of mercury intrusion porosimetry, micro-computed tomography, and nuclear magnetic resonance. In this way, we achieve much deeper insight into the pore space due to the different resolutions and sensitivities of the applied methods to pore constrictions (throats) and wide pores (pore bodies). We experimentally quantify pore aspect ratios and volume distributions within the two pore regions. We clearly observe systematic differences between three SIP relaxation types identified previously, and we can attribute the SIP peak relaxation times to measured characteristic length scales within our materials. We highlight selected results for a total of nine sandstones. It seems that SIP relaxation behavior depends on the size difference of the narrow pore throats to the wide pore bodies, which increases from SIP type 1 to type 3.

INTRODUCTION

Many approaches in geophysics and hydrogeophysics use the characteristic relaxation time of electrical low-frequency impedance spectroscopy, that is, spectral induced polarization (SIP) measurements, to derive information on hydraulic or transport-related properties (Börner et al, 1996; Hördt et al., 2009; Weller et al., 2016), such as the effective permeability (e.g., Binley et al., 2005; Weller et al., 2015) or the pore size distribution (Revil and Florsch, 2010; Florsch et al., 2014; Niu and Revil, 2016). Based on the theory of Schwarz (1962), which relates the low-frequency dispersion of colloidal particles in electrolytes to the particle sizes of the grains, there is an ongoing discussion on how to interpret and relate relaxation phenomena in electrolyte-saturated solid matter, that is, how the measured relaxation times of porous natural rock such as sandstone (Sst), tuffs, and limestone depend on characteristic length scales of their pore systems. Some researchers report power-law relationships between the electrical relaxation time and the modal pore throat size measured with mercury intrusion porosimetry (MIP) for their samples (e.g.,

Manuscript received by the Editor 13 February 2019; revised manuscript received 20 March 2020; published ahead of production 10 June 2020; published online 19 June 2020.
[1]Bundesanstalt für Materialforschung und -prüfung (BAM), Department of Non-Destructive Testing, Berlin, Germany and Technische Universität Berlin, Berlin, Germany. E-mail: sabine.kruschwitz@bam.de (corresponding author).
[2]Leibniz Institute for Applied Geophysics, Rock Physics & Borehole Geophysics, Hannover, Germany. E-mail: Matthias. Halisch@leibniz-liag.de; Raphael. Dlugosch@leibniz-liag.de.
[3]Bundesanstalt für Materialforschung und -prüfung (BAM), Department of Analytical Chemistry, Berlin, Germany. E-mail: carsten.prinz@bam.de.

Scott and Barker, 2003; Kruschwitz et al., 2010; Titov et al., 2010). Hence, in case of consolidated materials, such as sandstones or other natural porous media, the length scale along which relaxation occurs is assumed to be the radii of the pore system.

However, in all of these models, electrical low-frequency polarization is agreed to occur along the interface of charged surfaces of pores and the fluid therein, rather than through the bulk fluid (i.e., across the diameter of the pore). Considering this, the reason why a dependency of SIP relaxation times on the pore throat diameters (which are only measured with MIP) could still be observed (e.g., for type 1 and partly type 2 samples as classified in Kruschwitz et al., 2016) could be that for these materials the pore throat lengths are relatively equal in size compared with the pore throat diameters. This, however, has never been proven experimentally. On the contrary, many samples feature long SIP relaxation times although they have very narrow pore throats such as, for example, the type 3 samples as classified in Kruschwitz et al. (2016).

From an experimental viewpoint, it is still not clear whether it is the narrow or the wide pore system that controls the observed electrical low-frequency relaxation phenomena. This requires that we characterize the pore systems in greater detail than has been done with MIP thus far. Only a deeper understanding of the characteristic length scales present in a pore space will help us to understand the underlying cause of the measured SIP relaxation phenomena.

In this study, we follow a multimethodical approach based on a joint interpretation of MIP, micro-computed tomography (μ-CT), and nuclear magnetic resonance (NMR). Each method is sensitive to different pore space properties and has different spatial resolutions and sensitivities; thus, it would be beneficial to fully leverage their potential by integrating these analyses. Zhang et al. (2017, 2018) demonstrate an approach of how to relate and combine the cumulative distributions of the pore volume as a function of pore size using the same methods as in the present study. In this paper, however, we assume that MIP always provides a throat size distribution (TSD), whereas μ-CT and NMR provide the pore size (i.e., the mean pore body) distribution (PSD). We present a greater variety of nine sandstone samples compared to Zhang et al. (2018), who showcase their approach on the Bentheimer and Röttbacher Sandstone (Sst). Furthermore, we are able to distinguish different types of pore systems and relate them to SIP relaxation behaviors.

In the following, we first present the theoretical background of electrical relaxation in quartz-based solid porous matter and give an overview of the different sandstone samples and experimental methods used in this study. Subsequently, we explain the data processing procedures and how we bring together the data obtained from different sources. In the "Results" section, we compare our findings for SIP types 1–3 samples and highlight the systematic differences between their pore systems. Then, various influencing factors such as the spatial resolutions of our measurement methods, the representativeness of the sample volumes, and implications for the membrane polarization model as yet are discussed. At the end, we summarize the results and present conclusions.

THEORETICAL BACKGROUND

In this section, the theoretical background of low-frequency electrical polarization in solid porous media is described. Schwarz (1962) and Schurr (1964) express the relationship between electrical relaxation time τ and particle radius R for fixed-layer polarization around polystyrene spheres in ionic solutions as

$$\tau_S = \frac{R^2}{2\mu_S kT} = \frac{R^2}{2D_S}, \tag{1}$$

where k is Boltzmann's constant, T is the absolute temperature, μ_S is the mechanical mobility, and D_s is the diffusion coefficient of the involved ions in the fixed layer. Note that $D_s = \mu_S kT$ and is known as the Nernst-Einstein relation.

Kruschwitz et al. (2016) study this highly debated relationship between the SIP relaxation time τ and the dominant modal pore throat size D_{dom} from MIP (in this paper referred to as D_{MIP} as we compare in the following modal pore sizes from different analysis methods), for consolidated porous rock samples compiling the largest and most diverse data set yet. They worked with geologic materials from different areas with a wide variation of D_{MIP}, specific surface areas related to pore volumes (S_{por}), porosities (Φ), and permeabilities (k). The main goal of that study was to find the characteristic textural length scale controlling low-frequency relaxation and, hence, the frequency of the peak quadrature conductivity in a systematic way. In conclusion, Kruschwitz et al. (2016) divide the large group of samples into three (relaxation) types (see Figure 1). Figure 1a shows the measured peak SIP-relaxation times τ_{peak} as a function of D_{MIP}. The first subgroup ("type 1" samples) follows the "predicted" behavior (e.g., Scott and Barker, 2003) and feature τ_{peak} values that correlate with the TSD of the samples. A representative of type 1 samples is Udelfanger Sst (Figure 1b). The second subgroup ("type 2" samples) consists of rocks that likewise seem to follow the predicted $\tau_{\mathrm{peak}} \sim D_{\mathrm{MIP}}$ relationship, but at the same time show large τ_{peak} values (i.e., a low-frequency relaxation), which cannot be explained by the very small pore throat sizes measured with MIP. A representative of type 2 samples is Langenauer Sst (Figure 1c). These materials show a so-called "double-peak" SIP behavior; that is, they show two separate relaxation processes in the SIP data. They are characterized by two τ_{peak} values, whereas their pore systems feature only one D_{MIP}. Samples that belong to the third subgroup ("type 3" samples) do not follow the predicted $\tau_{\mathrm{peak}} \sim D_{\mathrm{MIP}}$ relationship at all, but they do show very slow SIP relaxation processes even though D_{MIP} are typically smaller than 5 μm. A representative of this group is Santa Fiora Sst (Figure 1d). Kruschwitz et al. (2016) show the best power law fit for all samples of SIP type 1 plus those τ_{peak} of type 2 can be related to pore throat sizes (the low τ_{peak} relaxations):

$$\tau_{\mathrm{peak}} = 3\mathrm{e}^{-4}\mathrm{s} * (D_{\mathrm{MIP}}/\mu\mathrm{m})^{2.5}. \tag{2}$$

Based on equation 1, for Langenauer Sst, for example, we would expect (additionally to the pore throat size) a second characteristic length of approximately 20–150 μm to explain the high relaxation time of approximately $\tau_2 = 5.3$ s (marked in Figure 1a). The same holds true for Santa Fiora Sst: We would expect to see a characteristic length scale of approximately 10–100 μm to explain the high relaxation time of approximately $\tau_1 = 3.5$ s (also marked in Figure 1a). These findings again raise the question on what factor controls the low-frequency relaxation time in porous solid media.

Bücker and Hördt (2013a, 2013b) are the first to implement the so-called membrane polarization theory in recent analytical modeling approaches. Based on the results of their parameter studies, they argue that primarily the length, not the diameter, of the narrow pore constrictions determine the polarization and, hence, the relaxation

time scale. The influence of the latter seems to be weak, if it is at all measurable (Bücker and Hördt, 2013b). The authors derive two analytic equations for each case, depending on the length ratios of the (mean) narrow and wide pore sizes. In addition, they argue that the total or effective relaxation will be dominated by the "shorter" one of the two and the diffusion coefficient in the particular part of the pore. Consequently, they postulate a "new" relaxation time for pore networks dominated by very short narrow pores (τ_{nSNP}):

$$\tau_{n\mathrm{SNP}} \sim \frac{\Delta L_2{}^2}{D_{p2}}, \tag{3}$$

with ΔL_2 being the length of the narrow pore and D_{p2} the diffusion coefficient of the cations in this pore. If the pore network is dominated by very long narrow pores, a different relaxation time (τ_{LNP}) dominates the effective polarization behavior:

$$\tau_{\mathrm{LNP}} \sim \frac{\Delta L_1{}^2}{D_{n1}}, \tag{4}$$

with ΔL_1 being the length of the wide pore and D_{n1} being the diffusion coefficient of the anions in the then "active" wide pore. This study was the first to distinguish and analytically explain two different relaxation time regimes, but the systematic experimental verification is still required. This very simple idea turns out to be somewhat challenging to prove in the laboratory because the most often used and widely accepted method to describe pore size distributions is MIP. However, MIP merely provides "pore entrance" size distributions, or in other words, TSDs. In this case, "size" means the diameter of the throat, not its length. Thus, validating the above theory requires finding materials in which the narrow pore size does not dominate the relaxation time and then postulating that for this material it is most likely the wide pore controlling the SIP relaxation time.

SAMPLES AND METHODS

In this section, the samples and different experimental methods used in the present study are described.

Samples

For our comparison of the pore space characteristics, six sedimentary rocks, two samples of each relaxation type, are selected for detailed presentation in the main part of this paper. Another three samples that we relate to relaxation type 1 are presented in Appendix A.

The two type 1 samples shown in the main text are Udelfanger ("Ud") Sst and Cottaer ("Cot") Sst (compare Figure 1a, marked in

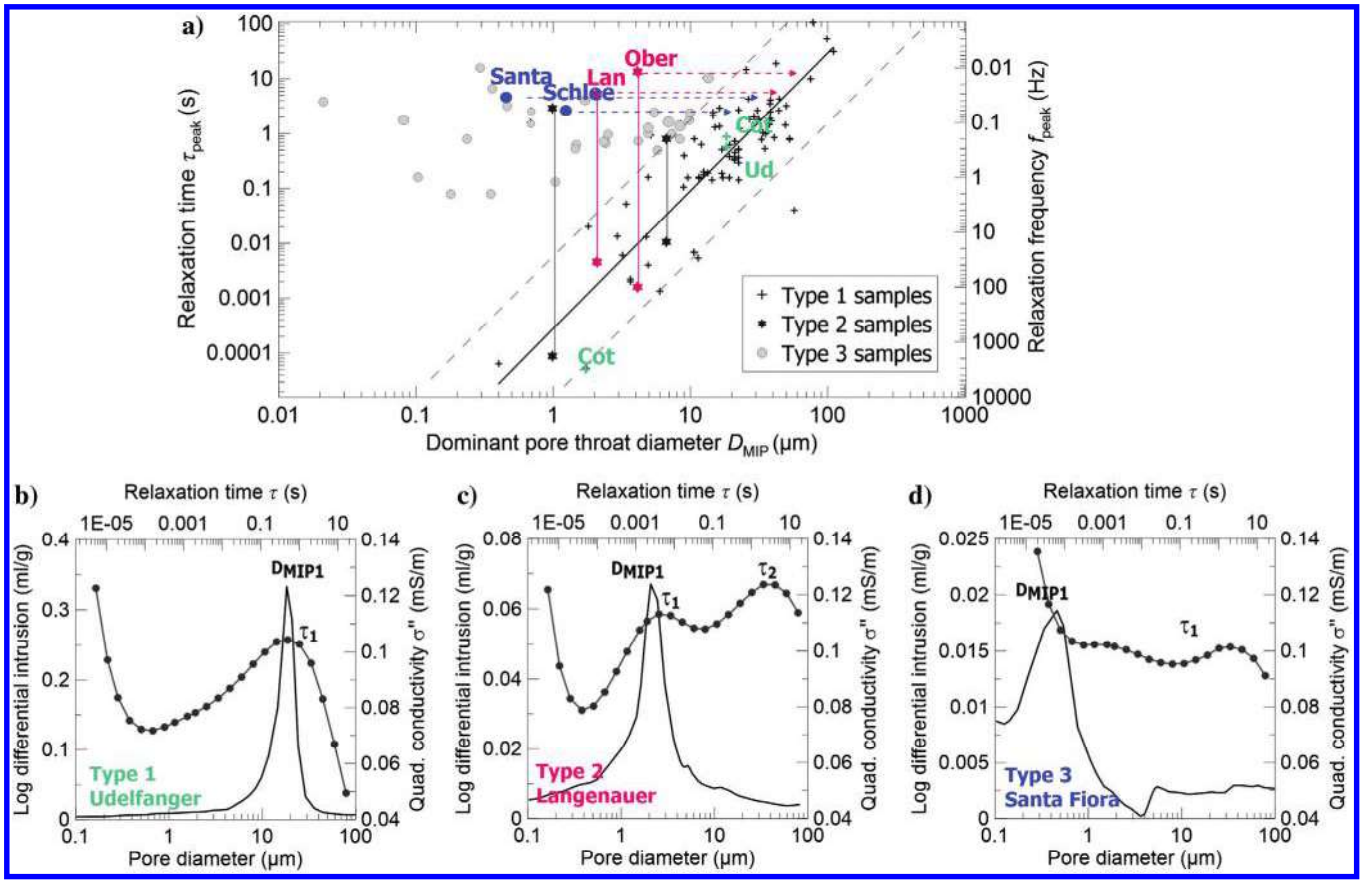

Figure 1. (a) SIP relaxation time versus dominant pore throat size of rock samples measured with MIP subdivided into characteristic types (after Kruschwitz et al., 2016). Best correlation for types 1 and 2 (equation 2; continuous line). Two representative samples of each type, which are discussed in the main part of the paper, are highlighted. (b-d) SIP (dotted line, bottom and left axes) and according MIP (solid line, top and right axes) curves for representative samples of each type; both x-axis are aligned using equation 2. Dominant pore throat sizes are marked with D_{MIP} and SIP relaxation times with τ.

green). Udelfanger Sst is of yellowish-gray color, fine grained and pored, well-sorted and homogeneous sandstone from the Middle Triassic. It is quarried near Trier in Rhineland Palatinate, Germany; it contains approximately 65% quartz, 22% rock fragments, 8% feldspars, 3% carbonate, and 2% muscovite; bonding varies between clayey, clayey-ferritic, and kaolinitic (Grimm, 1990). Grain sizes range between 0.01 and 0.15 mm, and average around 0.1 mm. Cottaer Sst deposits in the river Elbe valley in the Elbe Sandstone Mountains, Germany (Ehling, 2011). It is a layered Cretaceous sandstone containing 95% quartz, fragments of mica, and bands of coal and clay (kaolinite and illite). The color varies from whitish to yellowish-gray. The pore size usually ranges between 0.1 and 0.22 mm, roughly the grain size of fine to medium sand. The quartz grains are mainly siliceously bonded, but the rock also contains unevenly distributed amounts of the phyllosilicates illite and kaolinite, altered feldspars, and carbon elements.

For the type 2 group, we show Langenauer ("Lan") Sst and Obersulzbacher ("Ober") Sst (compare Figure 1a, marked in magenta). Langenauer Sst (sometimes referred to as Dlugopole or Wünschelburger Sst, compared to Ehling, 2011) originates from the Upper Cretaceous, and recent outcrops can be found in the vicinity of Dlugopole, a few kilometers south of Wroclaw, Poland (Silesia). It is a medium-grained, white-yellowish sandstone. It contains approximately 80% quartz and a high amount of 15%–20% (mostly kali-) feldspar. Minor components are heavy minerals (hematite) and clay minerals, mostly smectite. Obersulzbacher Sst is quarried near Kaiserslautern in Rhineland-Palatinate, Germany. It was deposited in the lower Rotliegend. It is a greenish-gray rock, fine- to medium-grained, containing approximately 52% quartz, 40% rock fragments, 7% feldspar, and 1% accessories with mostly clayey, ferritic, and kaolinitic bonding. It is a medium- to well-sorted rock with grain sizes between 0.2 and 0.5 mm without layering (Grimm, 1990).

Schleeriether ("Schlee") and Santa Fiora ("Santa") Sst are members of type 3 (compare Figure 1a, marked in blue). Schleeriether Sst outcrops near Schweinfurt in Lower Franconia, Germany. It is an olive-gray, fine grained, mainly homogeneous rock from the Lower Keuper (German: Lettenkolenkeuper, a carbonic formation preserving fossils from the Triassic). It contains, on average, approximately 79% quartz, 28% rock fragments, 5% plagioclase, 3% opaque ores, 2% accessories, and 2% alkali feldspars. Bonding is mostly by chloritic clay minerals. Grain contacts are mostly elongated, the grain crotches partly clay-filled and small pores as well as pore walls partly covered with authigenic chlorite. Grain sizes range between 0.1 and 0.3 mm, and pore sizes measure approximately 0.1–0.2 mm (Grimm, 1990). Santa Fiora Sst is a fine- to medium-grained (this means that the grain sizes range between 0.02 and 0.6 mm with an average dimension of 0.3 mm), pale-yellowish, light-brown to red Italian sandstone deposited in the Lower Tertiary period (Erica, 2009). It is quarried near Santa Fiora in the province of Grosseto in Tuscany, Italy. Santa Fiora is a calcareous sandstone, containing approximately 60% (micritic) calcite, 25% quartz, 13% alkali-feldspar and plagioclase, and 2% accessories such as Fe oxides and muscovite. Calcite is the cement binder of the rock.

Environmental scanning electron microscopy (ESEM) images of all nine samples are shown in Figure 2. It should be noted that only six of them will be discussed in the main part of the paper, whereas the results of other three are shown in Appendix A. These images give a qualitative impression of the complexity of the rock material and the according pore systems, quantified for this study by the combined assessment of permeability, NMR, and 3D μ-CT data. Nevertheless, many other ESEM images have been used for mineralogical and qualitative analysis of the rock samples. As can be seen, the pore systems of the investigated sample materials range from "porous and well connected" (Figure 2a–2d), over "porous and connected" (Figure 2e–2g) to "tight and poorly connected" (Figure 2h–2i). The commonality is that every sample features a distinct amount of clay and/or Fe-bearing minerals, which have impacts upon the nitrogen adsorption (Brunauer, Emmet, and Teller [BET]) as well as upon the NMR data as described below.

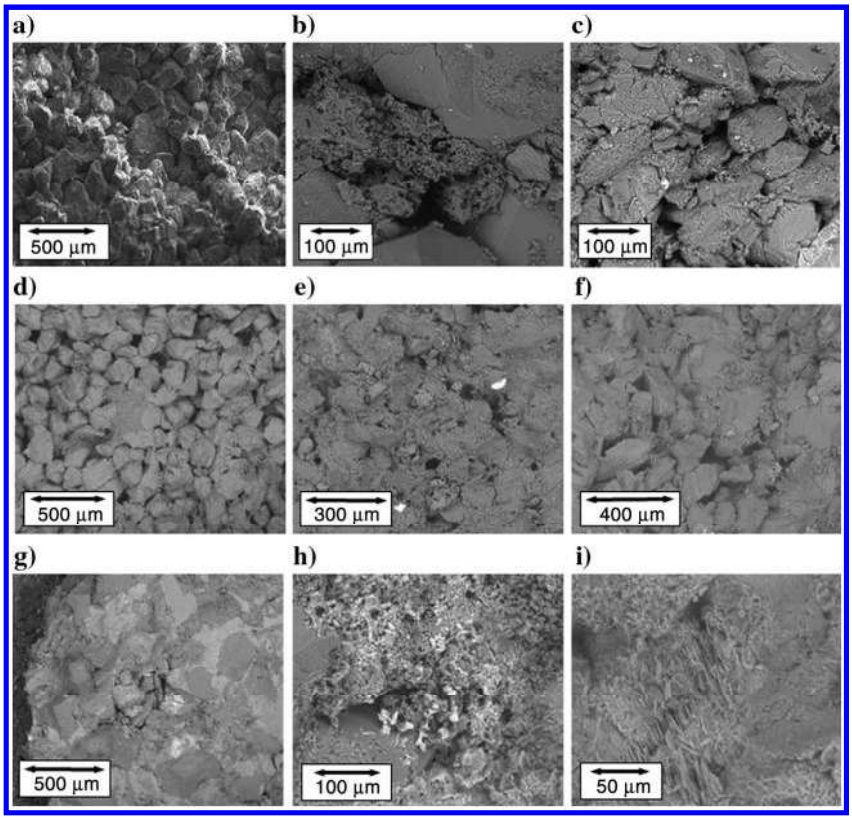

Figure 2. (a) ESEM images of Bentheimer Sst., (b) Langenauer Sst., (c) Udelfanger Sst., (d) Skala Sst., (e) Cottaer Sst., (f) Röttbacher Sst., (g) Santa Fiora Sst., (h) Obersulzbacher Sst., and (i) Schleeriether Sst.

Methods

Mercury intrusion porosimetry

Mercury intrusion porosimetry (MIP) measurements were conducted using an AutoPore III from Micromeritics (Norcross, USA). The pressure range of the AutoPore system from 4 kPa to 400 MPa corresponds to pore throat sizes of approximately 400 μm down to 3.6 nm. The cumulative intruded mercury

volume versus pressure curves were converted assuming cylindrical pore throats using the Washburn equation (Washburn, 1921; Bloomfield et al., 2001) resulting in pore TSDs. Note, however, that the volume attributed to the TSD is the volume that is accessed by overcoming the pore throat and not the actual volume of the pore throat. The actual volume of the throats would only have been measurable in additional MIP extrusion tests covering the entire pressure range of the former intrusion. The dominant pore throat sizes are the modal pore throat sizes and are calculated from the maximum value in the differential intrusion over pressure curves. For the MIP and BET tests that we sampled, the same sandstone blocks that we extracted the SIP and NMR samples from and assumed homogeneity.

Gas adsorption

Gas adsorption is a widely used method for determining the specific surface area. For determining the surface area, the amount of adsorbed gas is measured as a function of the relative pressure of the adsorptive. The specific surface area is calculated from the adsorption branch of the isotherm, using the approach of Brunauer, Emmet, and Teller (the so-called BET method, Brunauer et al., 1938). For the experiments, an ASAP 2020 device from Micromeritics was used and the isotherms were measured with liquid nitrogen at 77 K. In this paper, we use the specific surface area normalized to the pore volume (S_{por}). This value is often used in the literature to calculate the diameter of tubular pores (d_{Spor}), for example, to estimate NMR surface relaxivities (e.g., Keating and Falzone, 2013):

$$d_{\text{Spor}} = \frac{4}{S_{\text{Por}}}. \tag{5}$$

X-Ray μ-CT

The μ-CT imaging has been performed with a nanotom 180 S from GE Sensing and Inspection Technologies, a product line of phoenix|X-ray, a high-resolution (i.e., micron to submicron resolution) X-ray CT system. The minimum focal spot size is 0.6 μm, which is optimal for investigating small cylindrical samples with diameters of 1–2 mm and lengths of 5–10 mm. Following the same procedure as MIP, we extracted these cores from the larger sandstone blocks that we sampled for SIP and NMR. With these small μ-CT samples, we achieved voxel resolutions of 1.25–1.5 μm. The applied digital image analysis workflow is extensively described by Schmitt et al. (2016) and Halisch et al. (2016). For our analysis, we primarily worked with the equivalent pore diameter (EqD), which describes the corresponding diameter of a maximum inscribed sphere. The EqD is a frequently used structural descriptor in digital image analyses (e.g., Cnudde et al., 2011; Van Dalen and Koster, 2012): It is certainly more meaningful for regularly shaped pore systems compared with rather irregularly shaped ones in which the length versus width/breadth aspect ratios are high. During our μ-μ-CT data evaluation, we also determined the pore lengths, widths, and breadths and found that these lengths did not differ significantly from the EqD for any of our samples.

NMR

The NMR measurements were carried out with a Rock Core Analyzer from Magritek operating at a Larmor frequency of 2 MHz. We used a common Carr-Purcell-Meiboom-Gill (CPMG) pulse sequence (e.g., Dunn et al., 2002) with an echo spacing of 70 μs to monitor the transverse NMR relaxation (T_2). The built-in cooling/heating system ensures a constant sample temperature between 21°C and 22°C during the measurements. The porosity of the fully saturated samples (for NMR and SIP, the very same samples were used) has been determined by calibration with a bulk water sample of known dimension. The T_2-distributions are derived using a common multiexponential inversion approach. Hence, a regularization parameter is used, to weigh the minimum structure in the T_2-distribution and the minimum residual between the measured data and the model response (e.g., Whittall et al., 1991). During the inversion, we selected the smoothest model, which explains the data within the measuring error range. To simplify the T_2-distribution into a single value, we calculated the commonly provided logarithmic mean (e.g., Dunn et al., 2002). A logarithmically sampled PSD consisting of d_i is finally calculated assuming fast-diffusion T_{2i} in the ith cylindrical pore as follows (Brownstein and Tarr, 1979):

$$d_i = 4\rho T_{2i} \tag{6}$$

with d_i being the pore diameter of the ith pore and ρ being the surface relaxivity.

SIP

The SIP measurements were performed using a SIP-ZEL (Zentralinstitut für Elektronik) device (Zimmermann et al., 2008). The system allows for two simultaneous four-point measurements over a frequency range from 1 MHz to 45 kHz that we sampled with 27 logarithmically equidistant distributed measurements. The sample holder used has been described in Kruschwitz (2008). The spectra of the measured electrical conductivities (σ) consist of real (σ') and imaginary (also referred to quadrature) parts (σ''). We present in this paper only σ'' data of our samples because we want to examine the occurrence of τ_{peak} values and, as opposed to the SIP phase information, this quantity is mostly unaffected by the fluid properties. All of the shown SIP data are collected on samples that are fully saturated with NaCl brines of 0.1 S/m conductivity.

All samples in this study show a peak relaxation behavior, which means that the quadrature part of the electrical conductivity exhibits at least a single clear maximum at a certain frequency f, which corresponds to a certain relaxation time τ, which we refer to as the characteristic relaxation time τ_{peak}, that is, τ_1, τ_2 in the case of multiple maxima. It is calculated as the reciprocal value of the angular frequency ($\tau = 1/(2\pi f)$) at which the maximum quadrature conductivity is measured. As published in Weller et al. (2010), this maximum appears relatively independent of the pore fluid (type and) conductivity, which indicates that it is most likely controlled by specific textural properties of the pore space.

DATA PROCESSING

For the purpose of clarity, we chose a common representation of the results of all volume resolving methods, that is, MIP, μ-CT, and NMR, merged in one diagram. We plotted TSD for MIP and PSD for all other methods, that is, partial volumes for 30 log-spaced bins per decade of pore diameter because it is the common procedure for T_2 distributions. Whereas the volume presentation is natural for MIP, we resampled the irregularly spaced pressure stages of the

capillary pressure experiment using linear interpolation. In the case of μ-CT, the equivalent diameter distribution was adapted to 30 log bins per decade and the respective pore volumes were summed up. It should also be noted that the position of the PSD obtained by NMR and, hence, the surface relaxivity to transfer the T_2-distribution to PSD (see equation 6) has been chosen so that its maximum at large pores fits and mostly covers the PSD obtained by μ-CT. The SIP data are plotted in the same diagram, but we use separate x (τ) and y (imaginary conductivity) axes. We use the experimental fit (equation 2) presented in Figure 1 to correlate the bottom length-scale x-axis, used for MIP, μ-CT, and NMR, with the top SIP relaxation time x-axis used for SIP. We are aware that this fit, in its strictest sense, is only valid for the correlation of the τ_{peak} and D_{MIP}; this is also how we want the plots to be perceived: as a comparison of characteristic length scales in pore systems and dominant relaxation time peaks. We chose the minimum between the TSD from MIP and the PSD from μ-CT or NMR to estimate a cutoff pore diameter, hence, to distinguish between a wide and narrow pore system. Additionally, Appendix A presents for two samples a histogram of the relative frequency distribution (μ-CT counts) per pore diameter bin, another common form to present μ-CT data (Appendix B). This presentation is also remarkable because it demonstrates the existence and detectability of small pores using μ-CT. Nevertheless, this presentation is strongly weighted toward small pores, which may not contribute strongly to the total porosity depending on the particular pore system. In the following, we summarize our observations for two investigated sandstones for each type, respectively.

RESULTS

This section discusses the results obtained on six sandstones; these were investigated with the different experimental methods already presented. We begin with a presentation of the data for the SIP type 1 samples Udelfanger and Cottaer sandstone, followed by the results of the SIP type 2 samples Langenauer and Obersulzbacher sandstone, and we conclude with the SIP type 3 samples Schleeriether and Santa Fiora sandstone.

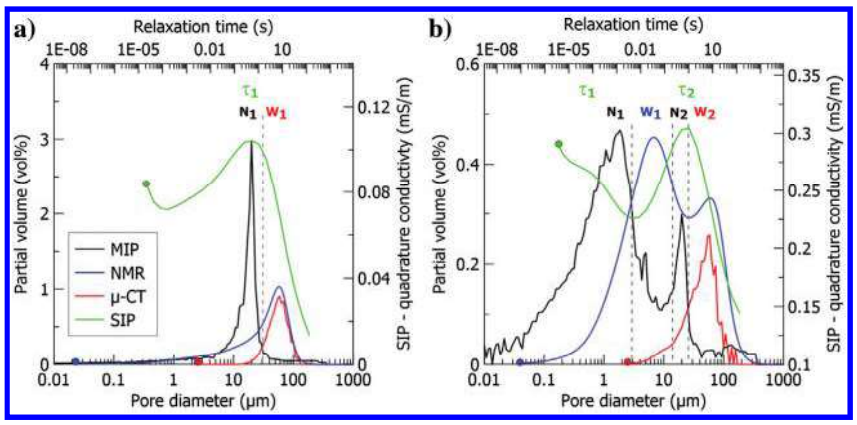

Figure 3. Pore volume distributions measured with MIP, NMR, and μ-CT (bottom and left axis) for (a) Udelfanger Sst and (b) Cottaer Sst. The SIP quadrature conductivity is plotted as a function of relaxation time (the top and right axis) using the fit in equation 2. Cutoff(s) between wide and narrow pore system(s) (the dashed line) and resolution limits of the methods (dots) are marked.

Type 1 samples

Udelfanger Sst (Figure 3a)

The SIP σ'' spectrum of Udelfanger sandstone features a single maximum at a characteristic relaxation time of ≈1 s, which is marked "τ_1" in Figure 3a. The TSD from MIP is narrow and unimodal with a dominant size of around 18.3 μm (marked "N_1"). Pore throats of this size well explain the position and shape of the SIP quadrature conductivity curve. Looking at the PSD from μ-CT, the biggest part of the total porosity seems to be affiliated to pores with an equivalent pore body diameter of approximately 60 μm (marked "W_1"). This results in a pore body (W_1) to pore throat (N_1) ratio of 3.3. Using a surface relaxivity of 50 μm/s, the PSD from NMR covers the PSD from μ-CT, but it additionally seems to be influenced by the smaller pore throat system. Using a cutoff pore size of 30 μm to distinguish between the N_1 and W_1 pores (as indicated by the gray dashed line in Figure 3a), the volume ratio of both systems obtained from NMR is 1:2.

Cottaer Sst (Figure 3b)

The SIP σ'' spectrum of the Cottaer sandstone is bimodal with characteristic relaxation times of ≈53 μs (τ_1) and ≈0.9 s (τ_2). The TSD from MIP c is likewise bimodal with peaks identifying pore throat sizes of 1.7 μm (N_1) and 18.3 μm (N_2). The unimodal PSD from μ-CT, however, indicates only one maximum of wide pore bodies of approximately 55 μm (W_2). Using a surface relaxivity of 100 μm/s, the PSD from NMR reasonably well covers the μ-CT result and at the same time suggests a second wide pore body regime at 6–7 μm (W_1). However, this second wide pore body regime is not resolved by the PSD from μ-CT as expected even though it is within the resolution limit of the method.

Altogether, the data imply that in Cottaer Sst, two pore networks exist, which can be distinguished by a cutoff length scale of 15 μm. For the first pore system, the ratio of pore body to pore throat size (W_1:N_1) results in approximately 3.8, and for the second (larger) pore system (W_2:N_2), it results in approximately 3. These size ratios are very small and are similar to what is observed in Udelfanger Sst. Assuming a cutoff pore size of 3 μm to distinguish between N_1 and W_1 and a cutoff size of 25 μm (as marked in Figure 3b by the gray dashed lines) to separate N_2 and W_2, we get 1:4 for the volume ratios of both pore systems from NMR.

Generally, for Type 1 samples, unrelated to the number of pore systems (here, one for Udelfanger and two for Cottaer Sst) present, we can conclude that we observe small ratios of pore throat to pore body sizes in the range of 3–10. Additional examples of type 1 samples are presented in Appendix A; these are Bentheimer, Skala, and Röttbacher Sst — compare Table 1.

Type 2 samples

Langenauer Sst (Figure 4a)

The SIP σ'' spectrum of the Langenauer Sst is bimodal and peaks at ≈4.5 ms (τ_1) and at 5.3 s (τ_2). The TSD from MIP identifies a majority of pore throats with a size of 2 μm. These very

small pores explain the fast SIP relaxation at τ_1, but not the slow relaxation at τ_2. Interestingly, the PSD from μ-CT identifies big pores in the range of approximately 70 μm. Assuming a surface relaxivity of 40 μm/s, the bimodal PSD from NMR supports both results. In contrast to the type 1 samples, the PSD from NMR assigns a significant volume to the pore throat system N_1; hence, it can be used to distinguish between W_1 and N_1. The size ratio between both pore systems ($W_1:N_1$) results in 35. Compared to the Udelfanger Sst, the pore system of Langenauer Sst is more heterogeneous and is clearly dominated by two very different length scales. The wide pore body size of approximately 70 μm convincingly explains the low SIP relaxation time (compared with Figure 1). Using a cutoff pore size of 10 μm to distinguish between N_1 and W_1 the volume ratio of both systems obtained from NMR is ≈1:1.

Obersulzbacher Sst (Figure 4b)

Another example of a type 2 material is Obersulzbacher Sst. Like Langenauer Sst, it shows two relaxation processes in the SIP σ'' spectrum: one at 16 ms (τ_1) and another one at 14 s (τ_2). The MIP result reveals only one modal throat size of 4.1 μm, which would explain the short relaxation time τ_1. In the PSD from μ-CT, we observe a majority of wide pores in the range of approximately 60 μm. The two pore systems identified by MIP and μ-CT are clearly supported by the NMR result, assuming a surface relaxivity of 60 μm/s. The size ratio between the wide and the narrow pore system (W_1:N_1) results in 15. Compared to Langenauer Sst, the PSD from NMR is clearly dominated by the smaller, narrow pore throats rather than by the wide pore bodies. This implies that a relatively big part of the porosity, that is, a bigger part than in the wide pore bodies, is contained in the throats. Using a cutoff size of 30 μm to distinguish between N_1 and W_1, the volume ratio of both systems obtained by NMR is ≈3.6:1.

Type 3 samples

Schleeriether Sst (Figure 5a)

Type 3 samples only show a slow relaxation in the SIP σ'' spectrum that cannot be related to the dominant pore throat measured with MIP. One example is Schleeriether SSt, which has a D_{MIP} of 1.2 μm plus a second maximum at 0.05 μm. However, the latter can probably be considered to be of minor importance because it would not affect the measurable SIP spectrum (because it would theoretically cause relaxation times ≪0.1 ms, which is equivalent to frequencies ≫10 kHz≫10 kHz; compare with Figure 1). The pore throat of 1.2 μm should theoretically lead to a τ_{peak} of approximately 0.1 ms, but the SIP spectrum only contains a relaxation at approximately 2.7 s. The PSD from μ-CT, however, reveals a narrow distribution of wide pore bodies peaking at 65 μm very well explaining the slow relaxation SIP peak. Assuming a surface relaxivity of 200 μm/s, the PSD from μ-CT and the TSD from MIP are convincingly covered by the bimodal PSD from NMR. The size

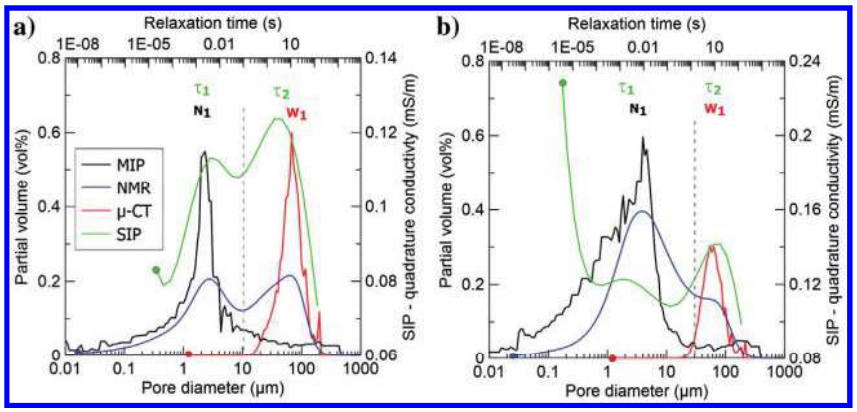

Figure 4. Pore volume distributions measured with MIP, NMR, and μ-CT (the bottom and left axis) for (a) Langenauer Sst and (b) Obersulzbacher Sst. See Figure 3 for further details.

Table 1. Summary of pore throat (N) and pore bodies (W) sizes along with pore aspect ratios and surface relaxivities ρ used for the NMR analysis, porosities obtained with the different methods, and specific surface area from N_2-adsorption measurements for all samples.

Sample	SIP type	D (μm)		Aspect ratio (-)	ρ (μm/s)	Porosity (vol%)				S_{por} (1/μm)
		N	W	W/N						
		MIP	μ-CT, NMR		NMR	3-weighing	NMR	MIP	μ-CT	BET
Udelfanger	SIP type 1	18.3	60.0	3.3	52	18.3	18.4	23.5	10.3	11.0
Cottaer		1.7/18.3	6.5/55.0	3.8/3.0	100	18.5	21.5	21.7	4.0	50.9
Bentheimer		38.8	125.0	3.2	65	23.8	22.7	23.8	18.4	2.8
Skala		29.0	90.0	3.1	40	26.4	25.7	24.8	17.3	2.2
Röttbacher		9.8	90.0	9.2	105	15.9	16.0	16.6	9.1	26.3
Langenauer	SIP type 2	2.1	70.0	35.0	40	12.0	12.8	12.0	6.9	35.6
Obersulzbacher		4.1	60.0	15.0	60	17.7	18.3	20.8	3.8	27.0
Schleeriether	SIP type 3	(0.05)/1.2	65.0	54.0	250	12.0	16.0	16.3	4.2	82.9
Santa Fiora		0.5	50.0	100.0	150	7.7	8.3	6.6	1.9	136.1

ratio of the wide to the narrow pore system is ≈54. When we use a cutoff size of 10 µm to distinguish both pore systems, we get a volume ratio of 1.5:1 based on the NMR.

Santa Fiora Sst (Figure 5b)

Another example of a type 3 material is Santa Fiora Sst. Interestingly, the SIP σ'' spectrum for this material slightly adumbrates a second maximum at approximately τ_{peak} of 1 ms, which is less distinct. Because the second maximum is minor, we classify Santa Fiora here as type 3. The TSD from MIP shows a unimodal distribution with a maximum at 0.5 µm bulging somewhat to the left. The PSD from µ-CT reveals a maximum of wide pores in the range of 50 µm. The size ratio between the wide and the narrow pore systems ($W_1 : N_1$) for Santa Fiora Sst is 100. Due to the fast NMR relaxation times, we choose a surface relaxivity of 150 µm/s. Whereas this did not link the maximum of the PSD from NMR to W_1 obtained by µ-CT, the obtained PSD is able to explain the MIP and µ-CT results. In this case, the PSD from NMR is dominated and mostly covers the pore volume contained in the narrow pore throats. Assuming a cutoff of 15 µm, the N:W volume ratio obtained from NMR is approximately 8:1.

For all of the presented samples, the important characteristic length scales measured with MIP, µ-CT, and NMR are summarized in Table 1. Also, the size ratios between the wide pore body and the pore throat are given as well as the surface relaxivity to convert the NMR result into a PSD. Our data clearly show that the size scale between the wide pore body and the narrow pore throat in the materials increases from SIP type 1 (<10) over type 2 (10–50) to type 3 (>50). This suggests that the pore systems actually get more heterogeneous or more extreme in the same order. Table 1 also presents the measured porosities obtained with triple weighing, NMR, MIP and µ-CT, the specific surface area from S_{por}, the modal pore throat diameter D_{MIP}, and the NMR mean log T_2-time (T_{2ML}) for all sandstones of this study.

DISCUSSION

In the following, we discuss the significant characteristics and limitations of our approach and findings. This comprises, the discussion of methodical parameters such as the spatial resolution limits of the experimental methods, our choices of NMR surface relaxivity values, and the representativeness of the data. We also discuss the implications for understanding the differences between the SIP types and on the membrane polarization model. Also, our findings are compared with those of other multimethodical approaches for pore space characterization.

Lowest spatial resolution limit

The methods used above differ in their spatial resolutions and limits of detection. To detect small pores with SIP, equation 2 implies that it is necessary to estimate the fast SIP relaxation times of a sample. This is challenging due to coupling effects, which often dominate the amplitudes of the recorded SIP data at fast relaxation times (e.g., see Obersulzbacher, Figure 4). Because it is very challenging to remove these coupling effects, we mark the highest measured SIP relaxation time in the presented spectrum. For measuring frequencies of up to 45 kHz ($\tau_{peak} = 3.5$ µs), and assuming equation 2, this leads to D_{MIP} of approximately 0.2 µm, which could impact the measured SIP data. Figure 1a also shows the relatively large scatter of the dependency SIP relaxation times on D_{MIP}, which could be the reason why the pore throats in Schleeriether Sst are not detected by the electrical measurements.

The spatial resolution of MIP depends on the highest applied pressure. For 400 MPa, this corresponds to pore throat sizes of approximately 3.6 nm. This is beyond the potential of SIP (and basically all of the other methods used in this work with the exception of gas adsorption) and is, therefore, beyond the presented TSD range.

For µ-CT, the smallest voxel size is 1.25 µm, but pores consisting of only one voxel are, for this study, regarded as unreliable and/or image processing noise. Provided that a significant contrast in the X-ray attenuation between the matrix and the pore space exists and the image quality is sufficient, the smallest reliable and resolvable pore size is 2.5 µm. However, the volume PSD obtained from µ-CT generally resolve only a few pore sizes <10 µm. Taking a closer look at a histogram presentation, that is, the number of detected pores per pore diameter (see Appendix B), it is obvious that these pores can be generally detected by µ-CT. However, their number seems to be significantly underestimated due to a reduced representativeness of the investigated 3D volume and, hence, of the detected pore sizes therein. This leads to an underrepresentation in the volume PSD, also indicated by the systematically lower porosity estimated by µ-CT (Table 1).

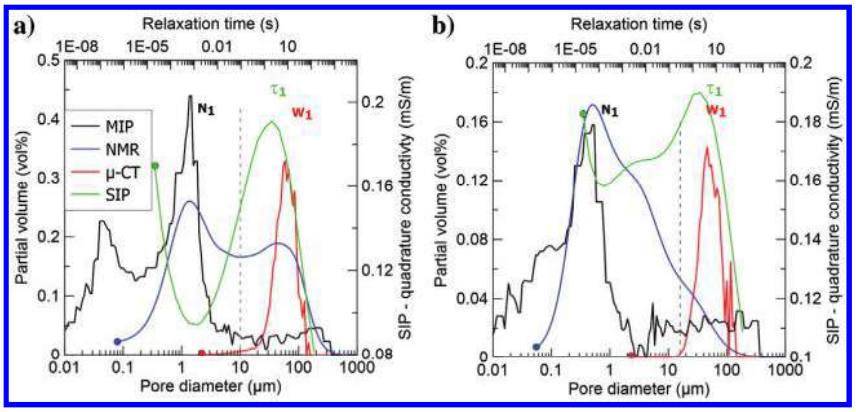

Figure 5. Pore volume distributions measured with MIP, NMR, and µ-CT (the bottom and left axis) for (a) Schleeriether Sst and (b) Santa Fiora Sst. See Figure 3 for further details.

To resolve small pores with NMR, fast relaxing NMR signals need to be detected. The ability primarily depends on the CPMG echo spacing and the achieved signal quality. Due to the short echo spacing of 70 µs and the generally high signal to noise ratio of several 100 to 1000, we assume that T_2-times >100 µs can be detected. The respective resolvable pore size, marked in the presented PSD obtained from NMR, depends on the assumed surface relaxivity (equation 6).

NMR surface relaxivity

NMR is a powerful tool to assess the pore space; however, a calibration, that is, estimation of the NMR surface relaxivity, is essential to transfer a T_2 distribution into a reliable PSD.

It is a common approach to use other petrophysical methods such as N_2-adsorption, MIP, flow measurements, and thin section imaging, but under certain circumstances, other NMR measurements can provide pore size information without calibration (e.g., Mitra et al., 1993; Müller-Petke et al., 2015).

We used the EqD-PSD from µ-CT to calibrate the NMR result for most samples because of the common sensitivity to the pore body size. The only exception was Santa Fiona Sst because doing so would lead to unreasonably high surface relaxivity values (i.e., >1000 µm/s) and large pores indicated by NMR, which were not resolved by µ-CT. In contrast to Zhang et al. (2018), however, we used the peak value of the PSD instead of a cumulative PSD. The reasons were to reduce the impact of a potential loss in representativeness of the volumes estimated by µ-CT, discussed in the following section, and the reduced significance of the PSD from NMR for pores with a low volume content, that is, the tail ends of the PSD.

For a general validation of the estimated NMR surface relaxivity values, quantitative mineralogical investigations have been carried out (X-ray diffraction, Riethfield analysis, and organic/anorganic carbon content). With this, a qualitative ranking of the impact of mineralogy upon NMR surface relaxivity has been derived (Table 2). It is known that clay minerals, as well as Fe-bearing minerals, increase the surface relaxivity values (Kleinberg, 1996; Kenyon, 1997; Keating and Knight, 2007). Accordingly, the estimated surface relaxivity values should be consistent with the derived rankings. In fact, the results confirm the estimated relaxivity values: The highest values can be found in the Cottaer, Santa Fiora, and Schleeriether samples. All of them feature a distinct amount of clay and/or Fe-minerals. In the case of the Santa Fiora sample, approximately 20% of calcite led to an increase as well. Lower relaxivity values can be found in samples with less to no clay and Fe-minerals, respectively.

To evaluate the absolute estimated NMR surface relaxivity values, it is important to note that this is a model parameter that simplifies the pore geometry and the complex characteristic of the pore surface (e.g., roughness) probed by NMR into a simple parameter. This parameter is somehow dependent of the resolution of the applied calibration method to sample the pore surface and is, therefore, in some papers referred to as the effective or apparent surface relaxivity (Kleinberg, 1996; Kenyon, 1997; Müller-Petke et al., 2015). The calibration of a PSD from NMR with another petrophysical method is reported to work well for MIP, flow measurements, centrifuge desaturation section imaging, and diffusion measurements (e.g., see Kleinberg, 1996; Kenyon, 1997; Dlugosch et al., 2013), methods that roughly sample the pore dimension. The reference values are 10–60 µm/s (section imaging and T_1 on sandstone, Kenyon et al., 1989), 30–300 µm/s (section imaging and T_1 on sandstone, Howard et al., 1993), 2.6–40 µm/s (NMR diffusion and T_1 on sandstone, Hürlimann et al., 1994), 120–320 µm/s (NMR diffusion and T_2 on sand, Müller-Petke et al., 2015), or 35–55 µm/s (flow measurements and T_2 on sand, Dlugosch et al., 2013). The mean pore radius d_{T2ML} estimated from T_{2ML} after calibration with µ-CT is presented in Table 3. It should be a known fact that N_2-adsorption has a high spatial resolution and is, therefore, very sensitive to pore roughness and clay content (e.g., Kenyon, 1997). Limiting the calibration of NMR to gas adsorption, that is, estimating a mean pore radius from BET (d_{Spor}) using equation 5, can lead to a significant underestimation of the pore radius by orders

Table 3. Summary of the NMR parameters of the samples and, hence, estimated "mean pore diameter" from NMR after calibration with µ-CT. Pore diameter from gas adsorption with BET analysis and factor d_{T2ML}/d_{Spor} for comparison.

	T_{2ML} (ms)	d_{T2ML} (µm)	d_{Spor} (µm)	d_{T2ML}/d_{Spor}
Sample	NMR	NMR	BET	NMR/BET
Udelfanger	110.0	23.0	0.36	63
Cottaer	26.0	10.0	0.08	132
Bentheimer	219.0	57.0	1.54	37
Skala	196.0	31.0	1.82	17
Röttbacher	41.0	17.0	0.15	113
Langenauer	44.0	7.0	0.11	63
Obersulzbacher	22.45	49.0	0.15	332
Schleeriether	4.9	4.9	0.05	102
Santa Fiora	2.5	1.5	0.03	51

Table 2. Cross-validation of estimated sample surface relaxivity ρ values with clay and Fe-mineral rankings based upon quantitative mineralogical investigations. ++ = major impact; −− = no impact; +− = average impact.

Sample	SIP type	Main component	Minor component	Clay ranking	Fe-mineral ranking	ρ (µm/s)
Udelfanger	SIP type 1	Quartz, dolomite	Kaolinite feldspar	+ −	+ −	50
Cottaer		Quartz	Kaolinite feldspar muscovite/illite	+ +	− −	100
Bentheimer		Quartz	Feldspar, kaolinite	+ −	− −	60
Skala		Quartz	Kaolinite	− −	− −	45
Röttbacher		Quartz	Feldspar, kaolinite, illite	++	+−	100
Langenauer	SIP type 2	Quartz	Kaolinite feldspar	− −	− −	40
Obersulzbacher		Quartz	Kaolinite feldspar muscovite/illite	+ −	+ +	60
Santa Fiora	SIP type 3	Quartz, calcite	Kaolinite feldspar muscovite/illite	+ −	+ −	150
Schleeriether		Quartz, feldspar	Kaolinite feldspar	+ +	+ +	200

of magnitude and, thus, the surface relaxivity by the same factor (see Table 3 and Appendix B).

Representativeness

The representativeness of the used samples also needs to be addressed. For example, in the case of Cottaer Sst, which is very inhomogeneous, it is possible that the selected volume for μ-CT was not representative and, therefore, that the second set of wide pores was not detected. Investigations of sister samples could help get better representative volume data. As an indicator for representativeness, porosity might be a useful parameter (Table 1). The μ-CT imaging is always limited by resolution and sample size. High resolution (approximately 1–2 μm voxel size) leads to a small sampled volume of a few cubic millimeters. Hence, the total porosity is always underestimated because small and very small pore features cannot be resolved and the loss in representativeness compared to other methods is larger (e.g., in the case of the Cottaer and Schleerither Sst). Accordingly, MIP samples are also very small compared with the samples used for NMR, SIP, and triple weighing (maximum 10 wt% of the original sample is used, i.e., approximately 2–5 g for each MIP run). Accordingly, variations on a millimeter to centimeter scale in the pore (throat) system cannot be resolved by a single MIP measurement, which will be addressed by ongoing research on this topic. In addition, we assume that the found "characteristic length scales," which are averaged values for all pores within the investigated volumes, are the "best fit" solution at this point of the research. We recognize that these values do not necessarily need to match the entire sample volume as investigated by SIP. To overcome this challenge, sufficient improvements for MIP and 3D imaging techniques are necessary for the future.

SIP type

Our approach of combining MIP, μ-CT, and NMR for the investigation of complex pore spaces clearly shows systematic differences between the samples of SIP relaxation Type 1, 2, and 3. Assuming that not only the larger pores as resolved by μ-CT, but all pores are about spherical, that is, the length, width, and breadth diameters are all about equal, we find that the SIP relaxation behavior of the samples present in a network is dominated by the size ratio of the narrow pore throats to the wide pores bodies. For the pore throats, this has always been a basic presumption, albeit certainly too simple; otherwise, we would not expect any correlation of τ and D_{MIP} at all because the polarization is expected to occur along the length of the pore areas not across their diameters.

For a small ratio of W/N, the SIP relaxation can be attributed to the narrow pore throats; although the body size is very similar and, in fact, the relaxation could, based on our results, just as well occur along the latter. When W/N becomes larger, we start to observe two SIP relaxations that can be attributed to the narrow and the wide pore system, respectively. When the size ratio gets very large, the slow relaxation process becomes dominant and the fast throat-related relaxation completely disappears.

Following this mindset, we assume that the relaxation processes along the two pores compete. Whereas for SIP types 1 and 2 samples we see relaxation along the narrow pores, it seems to disappear for SIP type 3 samples. Three possible explanations are conceivable (and maybe all three of them exist, depending on the properties of the pore system):

1) Relaxation effects along the very short and narrow pores might become small as the pores get quickly blocked and the diffusion coefficients become low (or are zero) in this zone.
2) Relaxation along the narrow pores might also remain existent, but get masked by EM coupling effects in the kHz/MHz frequency range. This would basically mean that SIP type 3 samples are similar to SIP type 2 samples, but the throat-related relaxation is not yet detectable with recent SIP laboratory equipment.
3) The assumption that the narrow pores are spherical might be wrong for type 3 samples. Because the length of the narrow pores (especially if they are <1–2 μm in diameter) cannot yet be measured with any method, we can only guess about their shape. It would also be conceivable that the narrow pores in these samples are very long so that relaxation along them appears at low frequencies (high τ_{peak}). In this case, the narrow pore relaxation would be superimposed by the relaxation along the wide pore.

It is indeed likely that all three phenomena can and will occur in real pore systems depending on their characteristics. For example, in the case of Santa Fiora Sst, explanation (3) seems the most convincing one. Though we do not have reliable numbers for the length of the narrow pores, we still get valuable indications from the NMR data. Using cutoff values based on MIP and μ-CT results, we can actually calculate from NMR the pore volume fractions allocated in the narrow and wide pore regions. The volume fractions we get for all of our samples (N:W in vol%) are reported in Table 4. Although we find usually bigger portions of the total pore volume in the wide pores for type 1 samples, we find it in the small pores for type 3 samples. This is consistent with a finding reported by Kruschwitz et al. (2016): In MIP extrusion experiments, a relatively bigger amount of intruded mercury remained in type 1 samples in so-called shielded pores (or wide pores behind narrow pores), whereas again for type 3 samples, only a small amount of shielded pore space was found. This might be an indication that in type 3 samples (or at least in Santa Fiora Sst) long narrow pores exist, which constitute a relatively large amount of the total porosity and cause a low-frequency relaxation along them.

Figure 6 shows a conceptual model drawing indicating the areas where we believe the polarization in materials of different SIP types is dominant: In the pore spaces of SIP type 1 samples, the narrow throats most likely control the relaxation. However, the wide pores are very similar in size and polarization may just as well occur along them (the τ_{peak}–D relationship has a high scatter, and as yet SIP cannot resolve the difference); in SIP type 2 materials the wide and the narrow pores are equally involved in the polarization process and the size difference of narrow and wide pores is large enough to differentiate two dominant relaxation times. In SIP type 3 samples, we seem to get polarization in the wide pore (at least for the materials investigated here), but it is conceivable that when the throats become short, polarization will also occur along them and cause a second high-frequency relaxation (making them actually SIP type 2 materials). Depending on the length of the throat, this polarization might occur at very high frequencies and get masked by EM effects.

Implications for the membrane polarization model

Hördt et al. (2017) investigate the geometric constraints of membrane polarization in an analytical form based on two cylindrical

pores (throats and wide pores) with different radii and lengths. The existence of two different pore sizes (narrow and wide) is a basic requirement of their model. They conclude from their parameter studies that relaxations in the wide pore regime (where elongated, rod-shaped pores dominate) are probably more relevant than those in the short narrow pore regime (where pores are rather spherical) because they produce higher phase shifts and the parameter range generating measurable phase effects is larger. As a result, they assume that the length of the wide pores is the characteristic length scale more likely controlling SIP relaxation phenomena. The authors are able to reproduce with their model "SIP type 1 behavior" when the size ratios between the length and the diameter of the narrow and the wide pores are moderate. In contrast, when the size ratios become large, they observe "SIP type 3 behavior." But, note here that the size or aspect ratio Hördt et al. (2017) examine is the ratio of the pore length to the pore diameter of each pore type (narrow pore and wide pore) and not the size ratio of the narrow to the wide pore as used in our study. Thus, when they discuss moderate aspect ratios, the pores (narrow and wide) of their model are more spherical. Similarly, when they speak about large aspect ratios, their pores are more elongated. In summary, according to their analytical model in both cases, the relaxation takes place along the wide pore.

The experimental data presented here do not directly support the findings of the analytical modeling approach presented by Hördt et al (2017) because as a first approximation (using the equivalent diameter in the μ-CT data analysis) the pores that we measure are spherical and therefore always have a moderate aspect ratio of approximately 1. We find instead that the size difference of dominant narrow and wide pores is, rather, controlling the relaxation. Moreover, we do not find any indication that SIP relaxation is more likely to occur in the wide pore. On the contrary, samples with intermediate aspect ratios (in our sense) show high-frequency relaxations that can be explained by the measured narrow pore size along with low-frequency relaxations that now can be attributed to the wide pore sizes.

Comparison to other multimethodical approaches for pore space characterization

Somewhat similar to our study, Müller-Huber et al. (2018) also combine NMR, MIP, and SIP for a better understanding of pore

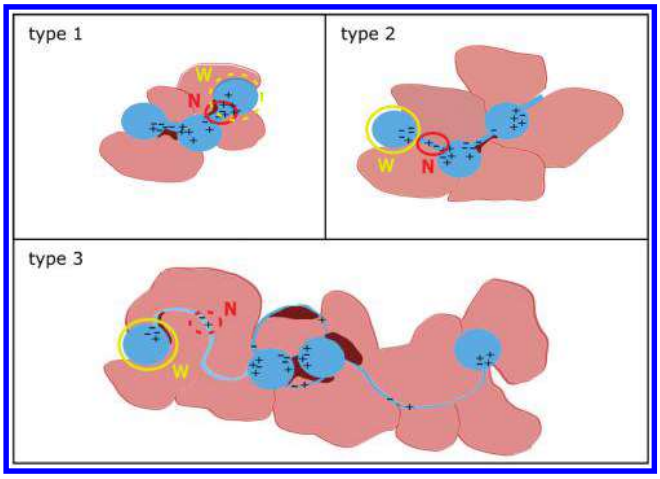

Figure 6. Conceptual model drawing indicating the areas in the pore space where polarization seems to be dominant for the three different SIP relaxation types (marked with the solid line). Polarization may as well occur along the areas marked with the dashed line, but it is as yet difficult to resolve with SIP. The aspect ratio W:N increases from type 1 to 3.

Table 4. Pore area, modal pore size in narrow and wide pore area, detected volumes with μ-CT, NMR, cutoff pore sizes, and volume ratios N:W as determined from NMR.

Sandstones	SIP type	Pore system	Modal pore size (μm)	Volume (vol%)		Cutoff (μm)	Vol. ratio
				μ-CT	NMR	NMR	N:W
Udelfanger	SIP type 1	N	18.3	—	6.0	30	≈1:2
		W	60.0	10.2	12.5		
Cottaer		N_2	18.3	0.4	1.9	25	≈1:4
		W_2	55.0	3.2	6.7		
		N_1	1.7	—	2.7	3	≈1:4
		W_1	6.5	0.4	10.3		
Bentheimer		N	38.8	—	7.8	60	≈1:2
		W	125.0	17.1	15.2		
Skala		N	29.0	—	13.0	45	≈1:1
		W	90.0	16.0	12.7		
Röttbacher		N	9.8	—	7.5	25	≈1:1
		W	90.0	9.0	8.5		
Langenauer	SIP type 2	N	2.1	—	6.0	10	≈1:1
		W	70.0	6.9	6.8		
Obersulzbacher		N	4.1	—	14.3	20	≈3.6:1
		W	60.0	3.7	4.0		
Santa Fiora	SIP type 3	N	0.5	—	7.4	15	≈8:1
		W	50.0	1.9	0.9		
Schleeriether		N	1.2	—	9.7	10	≈1.5:1
		W	60.0	4.1	6.4		

space features of different carbonate rocks. They use BET measurements to infer NMR surface relaxivities. In addition, they analyze (2D) SEM images to obtain more information on the size of the pore bodies (which are presumably dominating the NMR T_2 data). For their set of 10 carbonate rock samples, they report a decrease of the Cole-Cole relaxation time constant τ_{CC} with increasing pore body/pore throat ratio but no clear dependence of τ_{CC} on any one of the radii as such. To the extent that a direct comparison of the results obtained on sandstones, where the dependency of SIP relaxation times seems more pronounced, and carbonates is not possible in a straightforward way.

Very recently, Niu and Zhang (2018) present a joint inversion approach for SIP and NMR data with the aim of enhancing the characterization of pore spaces. In their model, the authors presume that MIP sufficiently describes the pore sizes of a medium and SIP and NMR are dominated by them. Our study in contrast shows that this might not be the case; instead, wide pores may play a significant role for the SIP and NMR behavior depending on their sizes and the relative amount of porosity that they encompass.

CONCLUSION

This study presents an important contribution toward a better understanding of SIP relaxation phenomena due to an enhanced characterization of complex pore systems in solid media using MIP, μ-CT, and NMR. We investigated nine samples belonging to three different types of SIP relaxation behavior. Our approach of jointly evaluating the data of this diverse data set was to reveal systematic differences in the pore spaces between the three groups.

The different applied methods each showed their advantages and disadvantages, which need to be considered to reliably and thoroughly characterize the pore space. MIP has the highest spatial resolution; thus, it is able to detect the size of the smallest pores reliably. Using μ-CT, we get information on the volume, pore aspect ratios, and pore size of the large pores (larger than approximately 2.5–10 μm). NMR is a useful tool to combine the information of MIP and μ-CT because it is sensitive to a wide range of pore sizes, that is, down to approximately 0.1–1 μm and provide pore volume information. However, an assumption in terms of the "calibration factor" surface relaxivity has to be made in order obtain pore size distributions. We achieved results consistent to MIP by calibrating our NMR relaxation time distribution using the equivalent diameter from μ-CT analyses.

As a result of our study, we found that the SIP relaxation behavior seems to depend on the size difference or aspect ratio of the narrow pore throats to the wide pore bodies. Samples of SIP relaxation type 1, which can be explained by a throat-related SIP relaxation time, show fairly uniform pore geometries, where pore throats and wide pores are quite similar in size. In these samples, tentatively more volume is attributed to the wide pore system (≈1 : 4) or is at least uniformly distributed (≈1 : 1).

Samples of SIP relaxation type 2 or 3, which feature long SIP relaxation times that cannot be explained by the narrow pore throat sizes, measured with MIP show more extreme pore size ratios. The investigated type 2 samples (Langenauer and Obersulzbacher Sst) are characterized by intermediate aspect ratios of narrow to wide pore sizes of 1:35 and 1:15. According to NMR, the pore volume is equally distributed or allocated to the narrow pore system (≈4 : 1)

For type 3 samples, which only feature long SIP relaxation times and no or no distinct narrow pore throat-related characteristic SIP relaxation time, we found the highest aspect ratios of wide to narrow pore sizes, that is, 1:54 for Schleeriether and 1:100 for Santa Fiora Sst. For these materials, a greater part of the pore volume tends to be in the narrow pore system.

Our results indicate that SIP polarization is most likely not restricted to the lengths of either narrow pore, that is, pore throats, or wide pore, that is, pore body, systems but can occur along both length scales. The aspect ratio of narrow to wide pore size seems to define which length scale effectively dominates the SIP relaxation. The relative amount of pore volume allocated in the narrow pore system tends to increase from SIP type 1 to 3 samples, but this is apparently not the crucial factor dominating the SIP relaxation behavior. Additionally, we are optimistic that a uniform SIP relaxation model can be found in future studies that can replace the categorization into different SIP types, but is only correlated to characteristic length scales of the pore space. However, we are convinced that only multimethodological studies, including awareness of the intrinsic resolution potential and limitations, can be successful to fully describe the complex pore space.

ACKNOWLEDGMENTS

The authors would like to thank S. Kaufhold and C. Ufer (Federal Institute for Geosciences and Natural Resources, Hannover, Germany) for the fruitful discussions about the qualitative and quantitative mineralogical composition of the investigated rock samples. A. Ehling (Federal Institute for Geosciences and Natural Resources, Hannover, Germany) provided us with additional mineralogic details for some of the sandstones used in this study. We are grateful to the anonymous reviewers for their constructive comments to improve the manuscript.

DATA AND MATERIALS AVAILABILITY

Data associated with this research are confidential and cannot be released.

APPENDIX A

ADDITIONAL TYPE 1 SAMPLES

Because we limit the main part of the paper on two samples for each SIP relaxation type, we show the result for three selected sam-

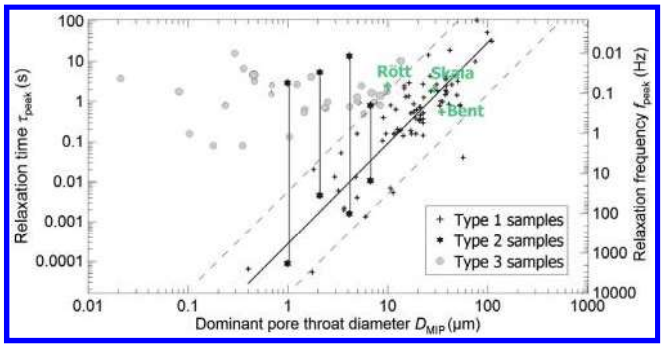

Figure A-1. SIP relaxation time τ_{peak} versus dominant pore throat size D_{dom} measured with MIP (after Kruschwitz et al., 2016). Three SIP type 1 samples are marked, for which the respective NMR, MIP, μ-CT volume distributions together with the SIP relaxation curve are shown in Figure A-2.

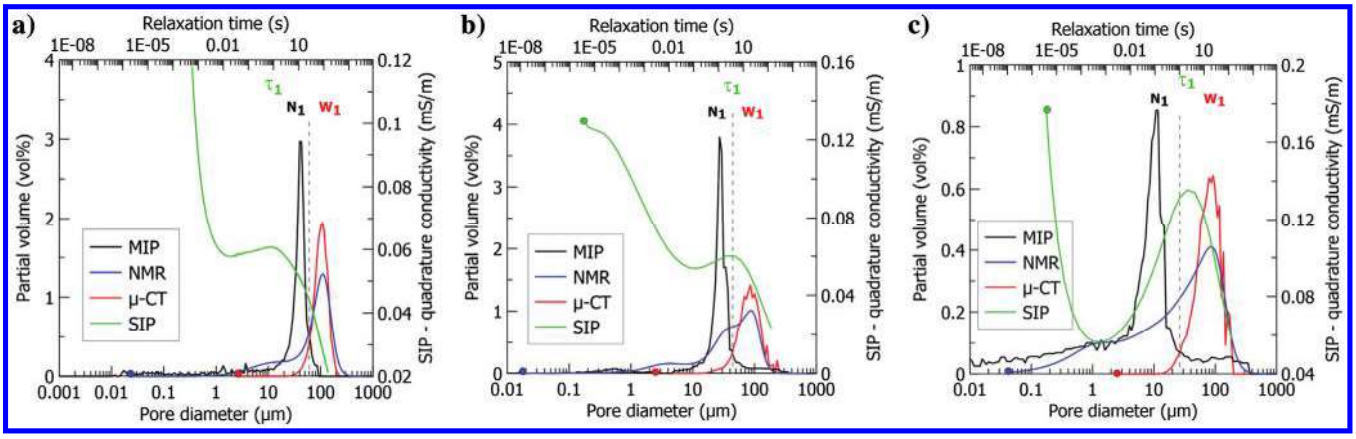

Figure A-2. Pore volume distributions measured with MIP, NMR, and µ-CT (the bottom and left axis) for (a) Bentheimer Sst, (b) Skala Sst, and (c) Röttbacher Sst. See Figure 3 for further details.

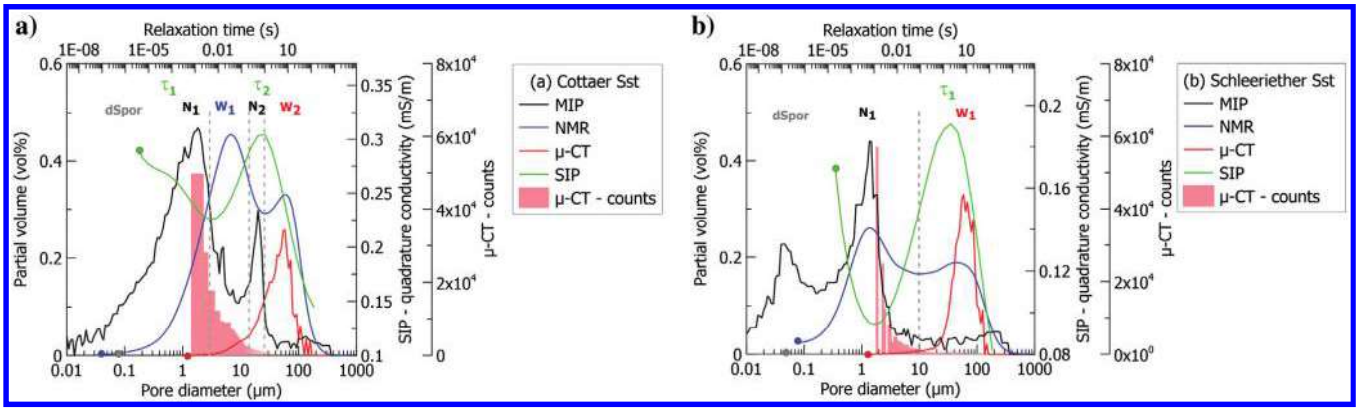

Figure B-1. Pore volume distributions measured with MIP, NMR, and µ-CT (the bottom and left axis) and number of pores detected with µ-CT in the respective pore size bin for (a) Cottaer Sst and (b) Schleeriether Sst. See Figure 3 for further details.

ples that belong to the common SIP type 1 group in Appendix A. Figure A-1 shows the location of these samples in a plot after Kruschwitz et al. (2016), which contrasts the SIP relaxation time versus the dominant pore throat size obtained from MIP. The results obtained by the full multimethod analyses consisting of SIP, MIP, µ-CT, and NMR are presented in Figure A-2 and Tables 1–4, respectively. As characteristic for type 1 samples, the pore throats and wide pores are quite similar in size and more volume seems to be allocated to the wide pore system.

APPENDIX B

ADDITIONAL µ-CT AND NMR ANALYSES

To keep the presentation of the multimethod analysis as simple as possible, we limited the µ-CT results in the main part of the paper to the volume-weighted histogram of the equivalent diameter distribution. However, there are some supposed conflicts between the PSD obtained from µ-CT and NMR as discussed in the paper. These are small pore systems, to which NMR attributes a significant part of the total volume, but which are hardly or not at all resolved by µ-CT. This is especially true for Cottaer Sst and partially for Schleeriether Sst. Looking at the count histogram obtained from the µ-CT measurement (Figure B-1), it is obvious that these small pore systems are detected by µ-CT, but the pore count; thus, the allocated pore volume seems to be heavily underestimated.

Additionally, the assumed surface relaxivity values, necessary to calibrate the PSD obtained from NMR, are generally highly discussed because they depend on the method used as the reference. We show the pore size estimated from S_{por} obtained from BET (equation 5) and contrast them with the PSD obtained from other methods (Figure B-1). This provides an intuitive evidence that at least for the samples presented in this work, BET was not an appropriate reference method of to calibrate the NMR T_2 distribution.

REFERENCES

Binley, A., L. D. Slater, M. Fukes, and G. Cassiani, 2005, Relationship between spectral induced polarization and hydraulic properties of saturated and unsaturated sandstone: Water Resources Research, **41**, W12417, doi: 10.1029/2005WR004202.

Bloomfield, J. P., D. C. Gooddy, M. Bright, and P. Williams, 2001, Pore throat size distributions in Permo-Triassic sandstones from the United Kingdom and some implications for contaminant hydrogeology: Hydrogeology Journal, **9**, 219–230, doi: 10.1007/s100400100135.

Börner, F., J. Schopper, and A. Weller, 1996, Evaluation of transport and storage properties in the soil and groundwater zone from induced polarization measurements: Geophysical Prospecting, **44**, 583–601, doi: 10.1111/j.1365-2478.1996.tb00167.x.

Brownstein, K. R., and C. E. Tarr, 1979, Importance of classical diffusion in NMR studies of water in biological cells: Physical Review A, American Physical Society, **19**, 2446–2453, doi: 10.1103/PhysRevA.19.2446.
Brunauer, S., P. H. Emmet, and E. Teller, 1938, Adsorption of gases in multimolecular layers: Journal of the American Chemical Society, **60**, 309–319, doi: 10.1021/ja01269a023.
Bücker, M., and A. Hördt, 2013a, Long and narrow pore models for membrane polarization: Geophysics, **78**, no. 6, E299–E314 doi: 10.1190/geo2012-0548.1.
Bücker, M., and A. Hördt, 2013b, Analytical modelling of membrane polarization with explicit parametrization of pore radii and the electrical double layer: Geophysical Journal International, **194**, 804–813, doi: 10.1093/gji/ggt136.
Cnudde, V., M. Boone, J. Dewanckele, M. Dierick, L. Van Hoorebeke, and P. Jacobs, 2011, 3D characterization of sandstones by means of X-ray computed tomography: Geosphere, **7**, 54–61 doi: 10.1130/GES00563.1.
Dlugosch, R., T. Günther, M. Müller-Petke, and U. Yaramanci, 2013, Improved prediction of hydraulic conductivity for coarse-grained, unconsolidated material from nuclear magnetic resonance: Geophysics, **78**, no. 4, EN55–EN64, doi: 10.1190/geo2012-0187.1.
Dunn, K. J., D. J. Bergman, G. A. Latorraca, K. Helbig, and S. Treitel, 2002, Nuclear magnetic resonance, petrophysical and logging applications: Pergamon.
Ehling, A., 2011, Schlesien — Mittelturon-Sandsteine im Heuscheuergebirge — Wünschelburger Sandstein, *in* A. Ehling and H. Siedel, eds., Bausandsteine in Deutschland, Sachsen-Anhalt, Sachsen und Schlesien (Polen): Bundesanstalt für Geowissenschaften und Rohstoffe, vol. **2**.
Erica (Technological Laboratory for Testing of Stones and Composite Materials), 2009, Test Report No. 1005 for Client Santafiora Srl. (unpublished document).
Florsch, N., A. Revil, and C. Camerlynck, 2014, Inversion of generalized relaxation time distributions with optimized damping parameter: Journal of Applied Geophysics, **109**, 119–132, doi: 10.1016/j.jappgeo.2014.07.013.
Grimm, W. D., ed., 1990, Bildatlas wichtiger Denkmalgesteine der Bundesrepublik Deutschland: Arbeitsheft 50 — Bayerisches Landesamt für Denkmalpflege.
Halisch, M., M. Schmitt, and C. P. Fernandes, 2016, Pore shapes and pore geometry of reservoirs rocks from μ-CT imaging and digital image analysis: Proceedings of the Annual Symposium of the SCA, SCA2016-093.
Hördt, A., K. Bairlein, M. Bücker, and H. Stebner, 2017, Geometrical constraints for membrane polarization: Near Surface Geophysics, **15**, 579–592, doi: 10.3997/1873-0604.2017053.
Hördt, A., R. Blaschek, F. Binot, A. Druiventak, A. Kemna, P. Kreye, and N. Zisser, 2009, Case histories of hydraulic conductivity estimation with induced polarization at the field scale: Near Surface Geophysics, **7**, 529–545, doi: 10.3997/1873-0604.2009035.
Howard, J. J., W. E. Kenyon, and C. Straley, 1993, Proton magnetic resonance and pore size variations in reservoir sandstones: SPE Formation Evaluation, **8**, 194–200, doi: 10.2118/20600-PA.
Hürlimann, M. D., K. Helmer, L. Latour, and C. Sotak, 1994, Restricted diffusion in sedimentary rocks. Determination of surface-area-to-volume ratio and surface relaxivity: Journal of Magnetic Resonance, Series A, **111**, 169–178, doi: 10.1006/jmra.1994.1243.
Keating, K., and S. Falzone, 2013, Relating nuclear magnetic resonance relaxation time distributions to void-size distributions for unconsolidated sand-packs: Geophysics, **78**, no. 6, D461–D472, doi: 10.1190/geo2012-0461.1.
Keating, K., and R. Knight, 2007, A laboratory study to determine the effect of iron oxides on proton NMR measurements: Geophysics, **72**, no. 1, E27–E32 doi: 10.1190/1.2399445.
Kenyon, W. E., 1997, Petrophysical principles of applications of NMR logging: The Log Analyst, **38**, 21–43.
Kenyon, W. E., J. J. Howard, A. Sezginer, C. Straley, A. Matteson, K. Horkowitz, and R. Ehrlich, 1989, Pore-size distribution and NMR in microporous cherty sandstones: Proceedings of the 40th Annual Logging Symposium, 24.
Kleinberg, R., 1996, Utility of NMR T2 distributions, connection with capillary pressure, clay effect, and determination of the surface relaxivity parameter rho 2: Magnetic Resonance Imaging, **14**, 761–767 doi: 10.1016/S0730-725X(96)00161-0.
Kruschwitz, S., 2008, Assessment of the complex resistivity behavior of salt affected building materials: Dissertation, Bundesanstalt für Materialforschung und -prüfung (BAM).
Kruschwitz, S., A. Binley, D. Lesmes, and A. Elshenawy, 2010, Textural controls on low frequency electrical spectra of porous media: Geophysics, **75**, no. 4, WA113–WA123, doi: 10.1190/1.3479835.
Kruschwitz, S., C. Prinz, and A. Zimathies, 2016, Study into the correlation of dominant pore throat size and SIP relaxation frequency: Journal of Applied Geophysics, **135**, 375–386, doi: 10.1016/j.jappgeo.2016.07.007.
Mitra, P., P. Sen, and L. Schwartz, 1993, Short-time behavior of the diffusion coefficient as a geometrical probe of porous media: Physical Review B, Condensed Matter, **47**, 8565–8574, doi: 10.1103/PhysRevB.47.8565.
Müller-Huber, E., F. Börner, J. Börner, and D. Kuhlke, 2018, Combined interpretation of NMR, MICP, and SIP measurements on mud-dominated and grain-dominated carbonate rocks: Journal of Applied Geophysics, **159**, 228–240, doi: 10.1016/j.jappgeo.2018.08.011.
Müller-Petke, M., R. Dlugosch, J. Lehmann-Horn, and M. Ronczka, 2015, Nuclear magnetic resonance average pore-size estimations outside the fast-diffusion regime: Geophysics, **80**, no. 3, D195–D206, doi: 10.1190/geo2014-0167.1.
Niu, Q., and A. Revil, 2016, Connecting complex conductivity spectra to mercury porosimetry of sedimentary rocks: Geophysics, **81**, no. 1, E17–E32, doi: 10.1190/geo2015-0072.1.
Niu, Q, and C. Zhang, 2018, Joint inversion of NMR and SIP data to estimate pore size distribution of geomaterials: Geophysical Journal International, **212**, 1791–1805, doi: 10.1093/gji/ggx501.
Revil, A., and N. Florsch, 2010, Determination of permeability from spectral induced polarization in granular media: Geophysical Journal International, **181**, 1480–1498, doi: 10.1111/J.1365-246X.2010.04573.X.
Schmitt, M., M. Halisch, C. Müller, and C. P. Fernandes, 2016, Classification and quantification of pore shapes in sandstone reservoir rocks with 3D X-ray micro-computed tomography: Solid Earth, **7**, 285–300, doi: 10.5194/se-7-285-2016.
Schurr, J. M., 1964, On the theory of the dielectric dispersion of spherical colloidal particles in electrolyte solution: The Journal of Physical Chemistry, **68**, 2407–2413, doi: 10.1021/j100791a004.
Schwarz, G., 1962, A theory of low-frequency dispersion of colloidal particles in electrolyte solution: Journal of Physical Chemistry, **66**, 2636–2642, doi: 10.1021/j100818a067.
Scott, J. B. T., and R. D. Barker, 2003, Determining pore throat size in Permo-Triassic sandstones from low-frequency electrical spectroscopy: Geophysical Research Letters, **30**, 1450–1453, doi: 10.1029/2003GL016951.
Titov, K., A. Tarasov, Y. Ilyin, N. Seleznev, and A. Boyd, 2010, Relationships between induced polarization relaxation time and hydraulic properties of sandstone: Geophysical Journal International, **180**, 1095–1106, doi: 10.1111/j.1365-246X.2009.04465.x.
Van Dalen, G., and M. W. Koster, 2012, 2D and 3D particle size analysis of micro-CT images: Proceedings of the Bruker micro-CT User Meeting, 1–16.
Washburn, E. W., 1921, The dynamics of capillary flow: Physical Review, **17**, 273–283, doi: 10.1103/PhysRev.17.273.
Weller, A., K. Breede, L. Slater, and S. Nordsiek, 2010, Effect of changing water salinity on complex conductivity spectra of sandstones: Geophysics, **76**, no. 5, F315–F327, doi: 10.1190/geo2011-0072.1.
Weller, A., L. Slater, A. Binley, S. Nordsiek, and S. Xu, 2015, Permeability prediction based on induced polarization: Insights from measurements on sandstone and unconsolidated samples spanning a wide permeability range: Geophysics, **80**, no. 2, D161–D173, doi: 10.1190/geo2014-0368.1.
Weller, A., Z. Zhang, L. Slater, S. Kruschwitz, and M. Halisch, 2016, Induced polarization and pore radius — A discussion: Geophysics, **81**, no. 5, D519–D526, doi: 10.1190/geo2016-0135.1.
Whittall, K. P., M. J. Bronskill, and R. M. Henkelman, 1991, Investigation of analysis techniques for complicated NMR relaxation data: Journal of Magnetic Resonance, **95**, 221–234, doi: 10.1016/0022-2364(91)90213-D.
Zhang, Z., S. Kruschwitz, A. Weller, and M. Halisch, 2018, Enhanced pore space analysis by use of μ-CT, MIP, NMR, and SIP: Solid Earth, **9**, 1225–1238, doi: 10.5194/se-9-1225-2018.
Zhang, Z., S. Kruschwitz, A. Weller, M. Halisch, and C. Prinz, 2017, Enhanced pore space analysis by use of μ-CT, MIP, NMR, and SIP: Proceedings of the 31st International Symposium of the Society of Core Analysts, SCA2017-086.
Zimmermann, E., A. Kemna, J. Berwix, W. Glaas, H. Münch, and J. Huisman, 2008, A high accuracy impedance spectrometer for measuring sediments with low polarizability: Measurement Science and Technology, **19**, 105603, doi: 10.1088/0957-0233/19/10/105603.